

## Supplemental Methods

### *Taxon selection*

Branchiopod crustaceans *Triops longicaudatus* (Order Notostraca) were grown according to the instructions from the commercially available Toyops' *Triops* kit until they reached maturity and desired size of 3-5cm at three weeks after hatching. All specimens were euthanized by refrigeration, being frozen for 3 hours, and then thawed in a refrigerator overnight.

### *Sediment collection and preparation*

Fresh estuarine sediment was collected from Belle Isle Marsh Reservation in Boston, Massachusetts. At low tide, one 5-gallon bucket of sediment was collected from each of the two 0.5-0.75 meters deep pits, one located one meter toward the stream from the peak of high tide (42.392208, -70.991179) and another 5 meters closer to the center of the tidal stream (42.392157, -70.991088). The sediment was collected from dark gray fine grain mud with a strong sulfidic smell, indicating the presence of sulfate-reducing bacteria in an anoxic environment. Large plant fragments and live organisms were manually discarded to remove excess organic matter. Sediment was mixed with artificial seawater (Instant Ocean®, Aquarium Systems), passed through a 2 mm sieve to remove remaining pieces of plant matter, shells, and organisms. Sieved sediment was placed into sealed containers with 100 mL of additional artificial seawater to create a thick slurry. A small sample of the sieved sediment was analyzed for bulk organic carbon content by weight. The organic carbon content of the sediment was 3.4%, measured by decarbonation with HCl and comparing dried sample mass before and after combustion of the organic matter<sup>1</sup>.

A loosely lithified smectite (clay mineral) was provided by Robert Gaines (Pomona College, California), collected in 2008 from Fish Creek Wash in Anza Borrego Desert State Park, Imperial County, California under research permit to Robert Gaines, Pomona College. The wash

primarily drains Plio-Pleistocene deposits of the Colorado River delta<sup>2,3</sup>. a large depression adjacent to the main wash during a high flow event collected the fine-grained clay smectite. X-ray diffraction analysis of oriented clay separates indicates that the clay is comprised primarily of illite with subordinate smectite and a negligible organic carbon content (Robert Gaines, personal communication).

The sediment enriched in sulfate-reducing bacteria and the clay minerals were mixed at a ratio of 1:3 by weight to produce a fine grain sediment with less 1% organic carbon by weight but with the natural bacteria population from the marsh sediment. The resulting mixture was 0.65% organic carbon by weight (Supplemental Table). Organic carbon was measured using a basic geochemistry/carbon isotope technique, taking a small sample of sediment, decarbonating it with HCl, drying the sample, identifying the ratio of carbon to nitrogen in the sediment and directly measuring the amount of nitrogen in the sample and calculating the carbon percentage based on the ratio<sup>1</sup>.

#### *Vial preparation*

Anoxic seawater was produced by boiling spring water in a flask with a septum and two needles while inputting nitrogen gas in one septum needle which was then used to make artificial seawater and set aside before adding the 0.5mM iron(ii) chloride solution in a dysoxic glove bag. The experimental vials were also prepared for the experiment inside a glove bag filled with dinitrogen gas to create a dysoxic, low oxygen, environment.

#### *Triops micro-CT scanning*

To create a morphological comparison scan, one *Triops* specimen was euthanized by submersion in 95% ethanol, stained in a solution of 1% iodine metal and 100% ethanol, left overnight, and

rinsed with 100% ethanol<sup>4</sup>. The iodine-stained specimen was wrapped in synthetic cotton batting in a plastic vial with 100% ethanol in Bruker SkyScan 1173 micro-CT scanner at the Digital Imaging Facilities (DIF) in the Museum of Comparative Zoology (MCZ) with voltage of 100kv, wattage of 80uA, 1mm Al filter, exposure of 750 ms, 0.3 angle degree step, and voxel size of 10.088  $\mu\text{m}$ . The scans were reconstructed as TIFF stacks in NRecon (Bruker Corporation) and visualized using the software Dragonfly 2019 4.0 (Object Research Systems, Montreal, Canada) (Fig. 2D).

#### *Data analysis and visualization*

Scans were reconstructed as TIFF stacks in NRecon (Bruker Corporation). Reconstructions used a variety of post-scan settings, unique to each scan comparing with fine tuning within the program to maximize reconstruction quality, generally with ring reduction of 1, smoothing of 1, and misalignment compensation between -7 and 7.

#### *Character selection and description*

Following the completion of scans through week 64, imaging of each vial was placed in a time series for comparison across the experiment (Supplemental Fig. 1-10). Images and videos of the three-dimensional volume renderings with the sediment removed were taken in Dragonfly from different perspectives to identify life position and three-dimensional orientation (Supplemental Video). Tomographic slices were also analyzed for detail and animated GIF image files were produced to have video of virtually slicing through the vials to identify fine morphological detail such as limbs and mandibles. Morphological characters were selected to prioritize comparison with previous studies (life position and morphology) and presence of changes uniquely available to this methodology (carcass and sediment density changes due to decay).

Character selection for Figure 18 was based on trackable changes in density using comparable LUTs in Dragonfly and tomographic slices. Changes in vials were tracked week to week and across vials each week (Supplemental Table, Supplemental Fig. 1-10). Ultimately, the carcass-based characters chosen were terminal bubble, cavity homogeneity, reduction in carcass density, cavity bubble; the sediment-based characteristics were bubble homogeneity, compression of bubbles, very light material, and dense material.

The morphological characters in Figure 19 were selected based on observability in the volume renderings, for example no internal tissues were recorded because no internal tissue staining was in the protocol. Results were compared to the unpublished PhD thesis of Dr. Thomas Hegna<sup>5</sup> on the decay of *Triops*, and the study by Butler et al.<sup>6</sup> on *Artemia salina*, a closely related taxon. Though *Artemia* has a more fragile constitution and thus decays faster than *Triops*, the former represents a useful reference point for interpreting the results of this project. For the morphological characters of *Triops* not present in *Artemia* such as the different carapace configuration and caudal furcae, descriptions of overall cuticle integrity and imaging of the terminal end and telson were used.

For the synthesis of Figure 10, published studies were selected for comparable taxa without biomineralized exoskeletons and methods that were representative of traditional decay experiments. Life position is defined as the overall integrity of the shape of the body wall, head and limb positions being like the animal in life for this study. In Butler et al.<sup>6</sup>, loss of life position was defined when the replicate reached what the authors defined as stage 4: “shrinkage of cuticle and internal structure, loss of some distal appendages.” In Selly and Schiffbauer<sup>7</sup>, loss of life position is defined when the authors describe the exoskeleton as disarticulated. Briggs and Kear<sup>8</sup> defined life position as when the carcass was described as disarticulated or decay stage 4. The life



position of the shrimp and stomatopod from Klompmaker et al.<sup>9</sup>, and the *Triops* in Hegna's thesis<sup>5</sup> were determined based on photos provided in the manuscript and descriptions of body articulation.

## References

1. Craig, H. The geochemistry of the stable carbon isotopes. *Geochimica et Cosmochimica Acta* **3**, 53–92 (1953).
2. Dorsey, R. Stratigraphy, tectonics, and basin evolution in the Anza-Borrego Desert region. in 89–104 (2006).
3. Dorsey, R. J., Axen, G. J., Peryam, T. C. & Kairouz, M. E. Initiation of the Southern Elsinore Fault at ~1.2 Ma: Evidence from the Fish Creek–Vallecito Basin, southern California. *Tectonics* **31**, (2012).
4. Metscher, B. D. MicroCT for comparative morphology: simple staining methods allow high-contrast 3D imaging of diverse non-mineralized animal tissues. *BMC Physiol* **9**, 11 (2009).
5. Hegna, T. A. A Dissertation Presented to the Faculty of the Graduate School Of Yale University In Candidacy for the Degree of Doctor of Philosophy. (2012).
6. Butler, A. D., Cunningham, J. A., Budd, G. E. & Donoghue, P. C. J. Experimental taphonomy of *Artemia* reveals the role of endogenous microbes in mediating decay and fossilization. *Proc. R. Soc. B.* **282**, 20150476 (2015).
7. Selly, T. & Schiffbauer, J. D. X-Ray tomographic microscopy as a means to systematically track experimental decay and fossilization. *PALAIOS* **36**, 216–224 (2021).
8. Briggs, D. E. G. & Kear, A. J. Decay and mineralization of shrimps. *PALAIOS* **9**, 431 (1994).

9. Klompmaker, A. A., Portell, R. W. & Frick, M. G. Comparative experimental taphonomy of eight marine arthropods indicates distinct differences in preservation potential. *Palaeontology* **60**, 773–794 (2017).

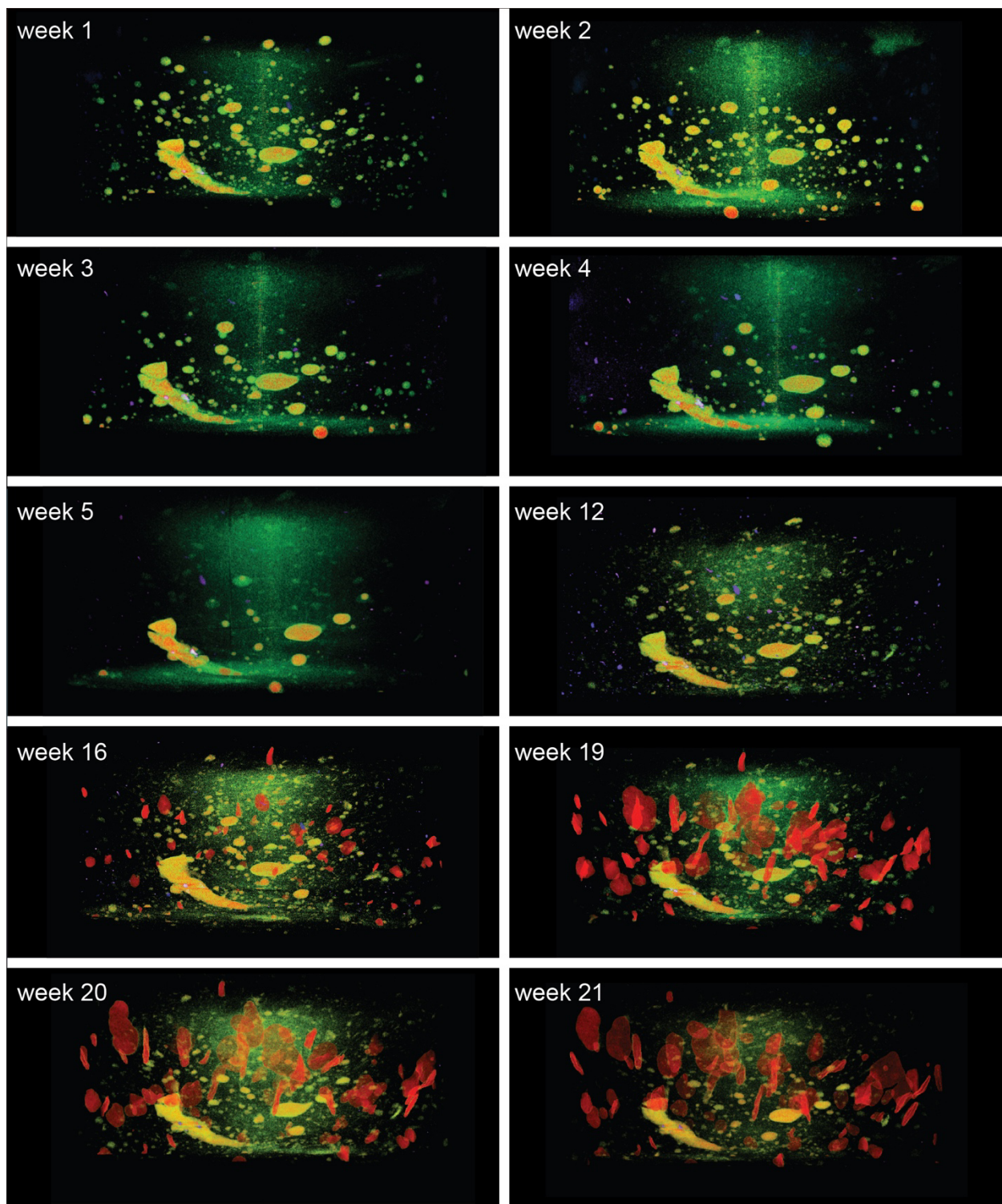


**Figure 1: Tomographic data of experimental vial A, weeks 1-21. Volume renderings of damaged carcass with pyrite inclusion.**

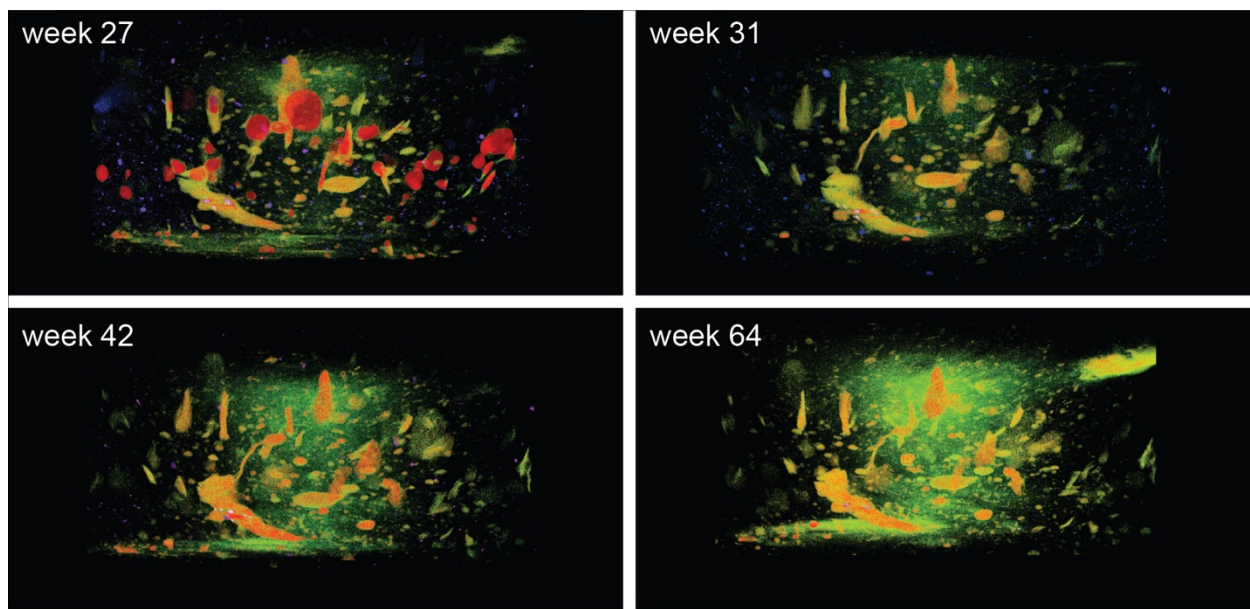


**Figure 2: Tomographic data of experimental vial A, weeks 27-64.** Volume renderings of damaged carcass with pyrite inclusion.



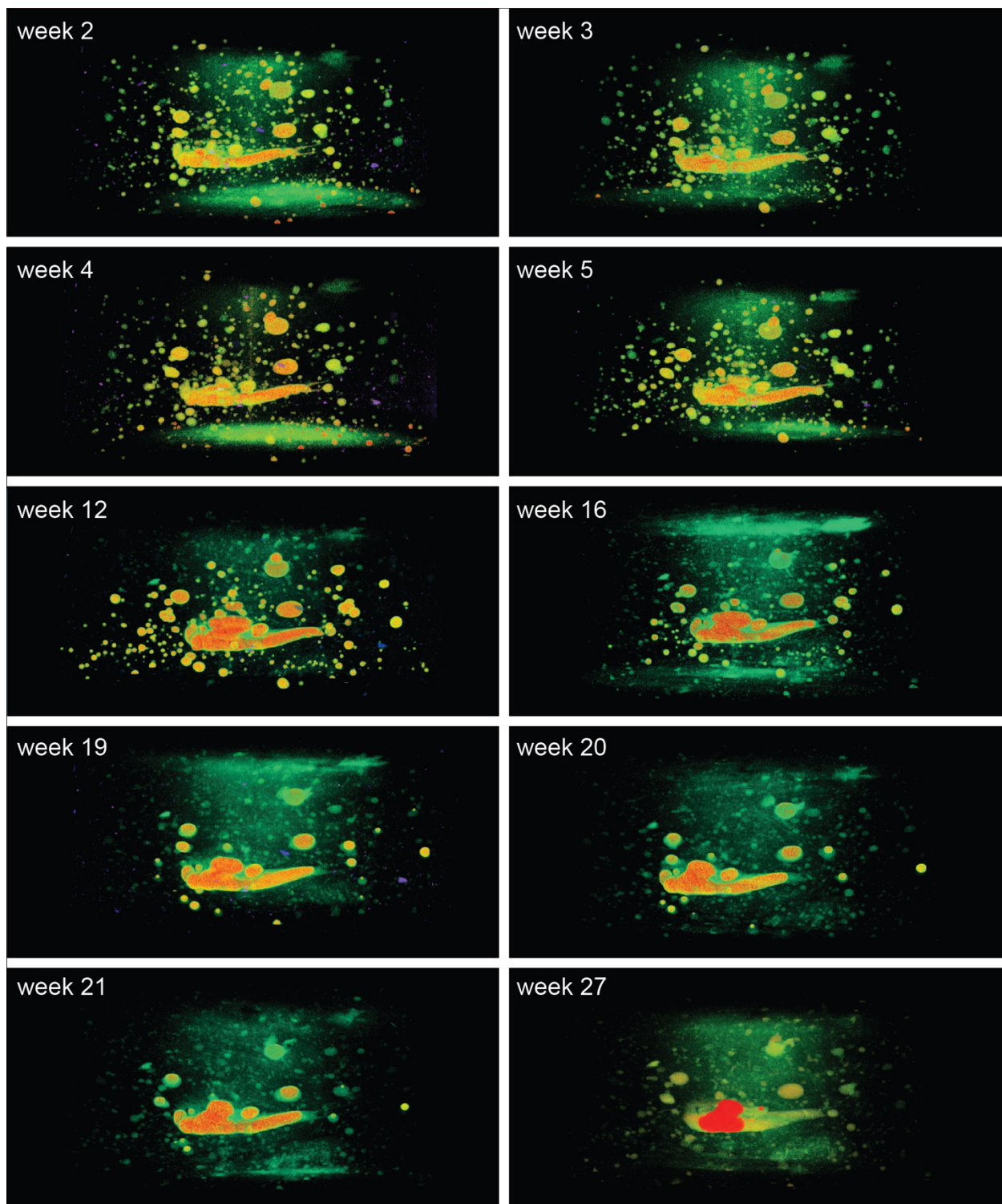


**Figure 3:** Tomographic data of experimental vial B, weeks 2-27. Volume renderings of damaged carcass with pyrite inclusion.

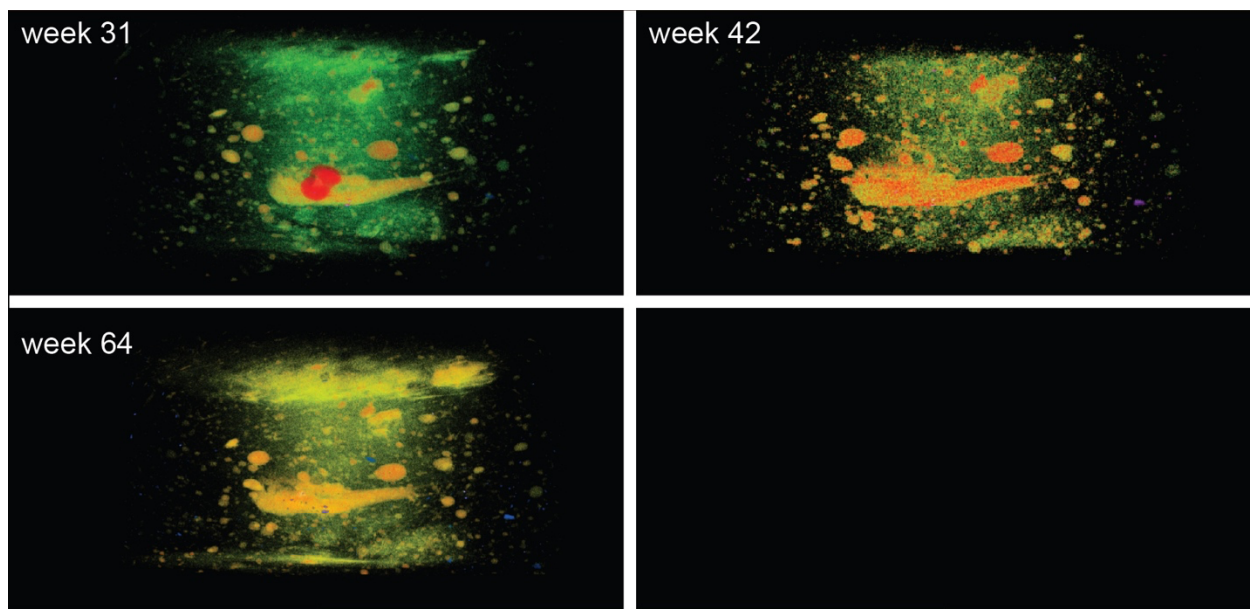


**Figure 4: Tomographic data of experimental vial B, weeks 31-64.** Volume renderings of damaged carcass with pyrite inclusion.



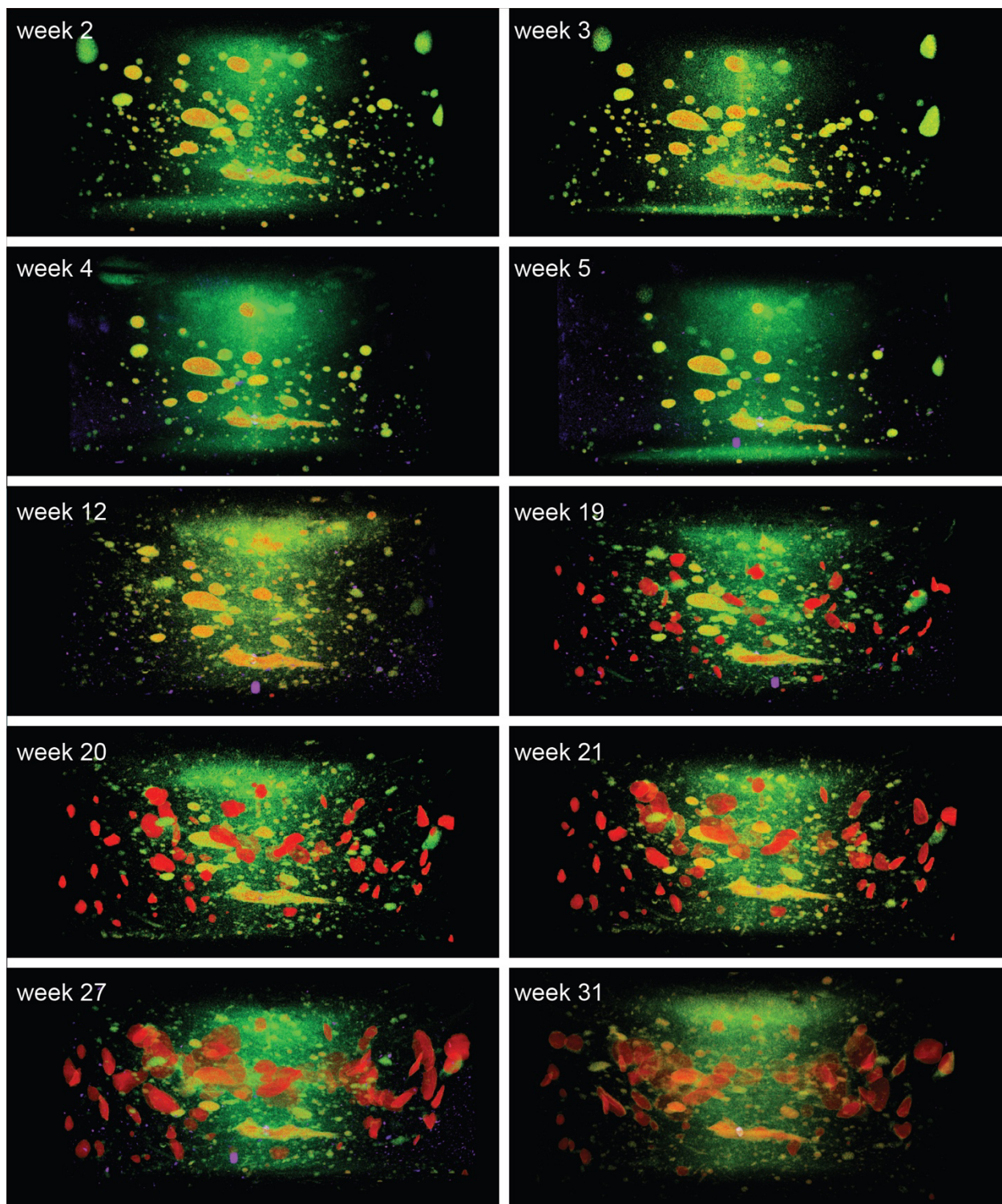


**Figure 5:** Tomographic data of experimental vial C, weeks 2-31. Volume renderings of damaged carcass with pyrite inclusion.

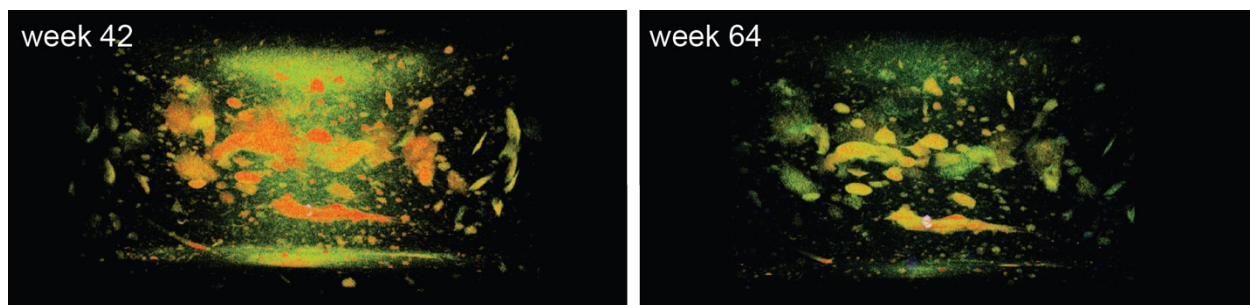


**Figure 6: Tomographic data of experimental vial C, weeks 42 and 64.** Volume renderings of damaged carcass with pyrite inclusion.



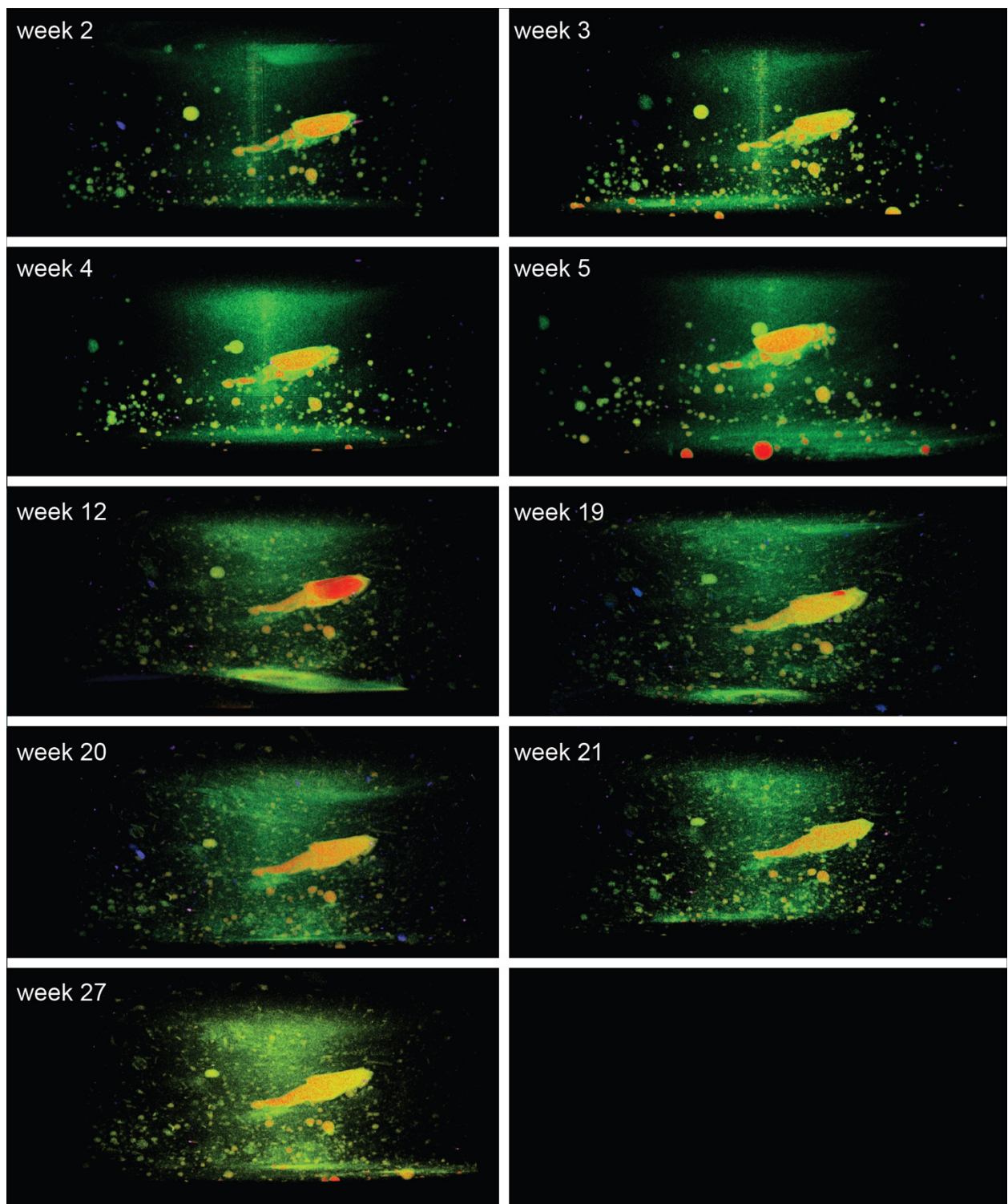


**Figure 7: Tomographic data of experimental vial D, weeks 2- 27. Volume renderings of undamaged carcass.**

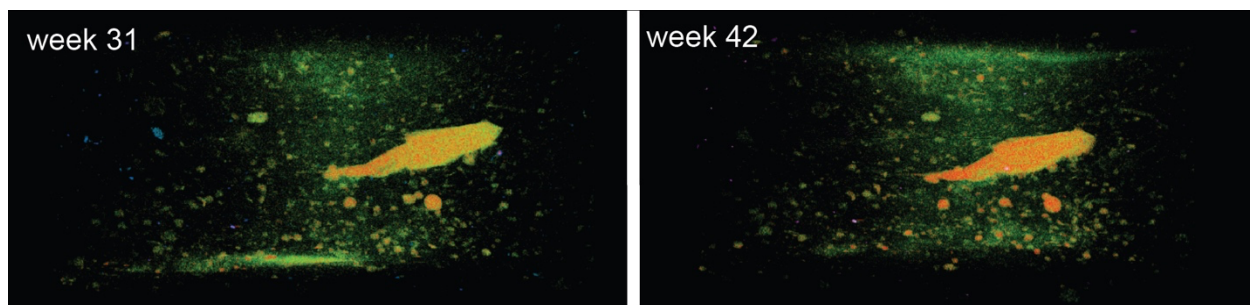


**Figure 8: Tomographic data of experimental vial D, weeks 31 and 42.** Volume renderings of undamaged carcass. Vial D was opened after week 42.

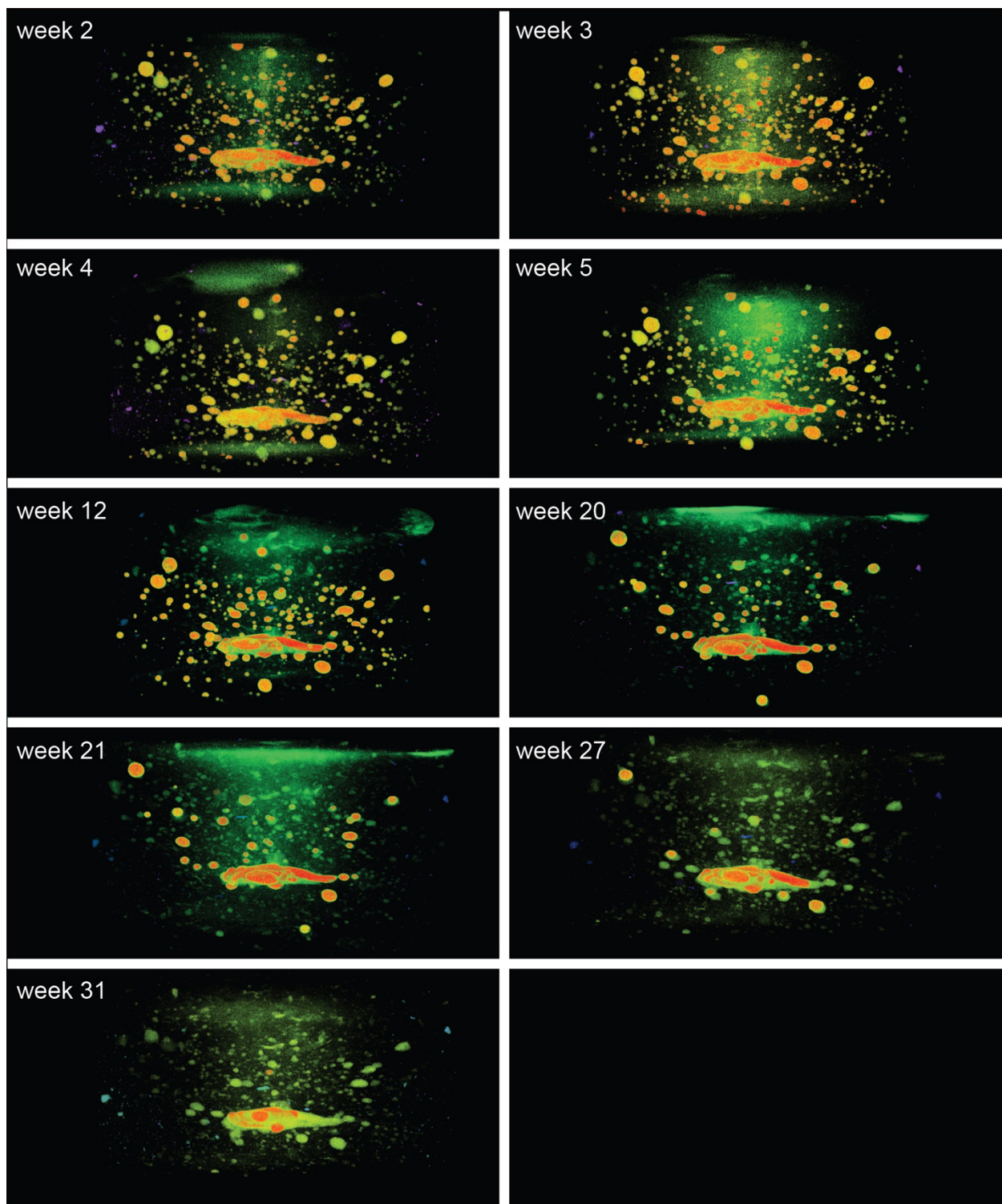


**Figure 9:** Tomographic data of experimental vial E, weeks 2-31. Volume renderings of undamaged carcass.

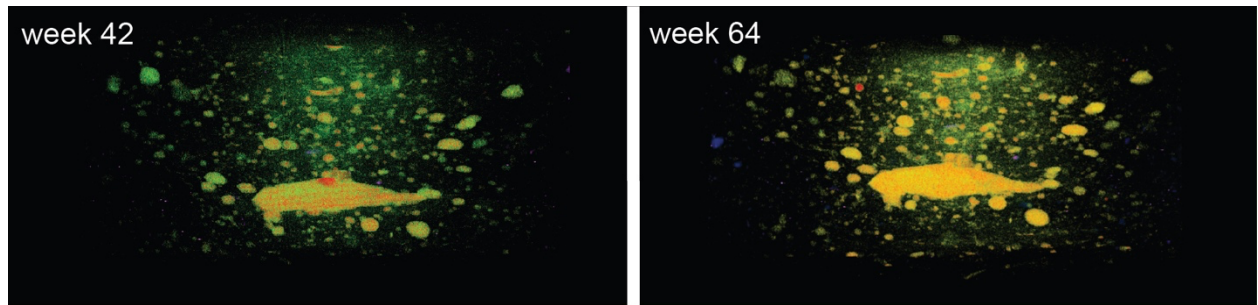


**Figure 10: Tomographic data of experimental vial E, weeks 42 and 62.** Volume renderings of undamaged carcass.

**Table: Observations of experimental vials and Organic Carbon Measurement Data**

**Video 1: Tomographic data of vial I, weeks 2, 20, 42, and 64.** Volume rendering and tomographic slices.

[https://www.dropbox.com/s/7meu6pc5c1cz67v/4\\_SupplementaryVideo.mp4?dl=0](https://www.dropbox.com/s/7meu6pc5c1cz67v/4_SupplementaryVideo.mp4?dl=0)